RSC Advances

ROYAL SOCIETY OF CHEMISTRY

www.rsc.org/advances

Cite this: DOI: 10.1039/c0xx00000x

www.rsc.org/xxxxxx

ARTICLE TYPE

Microwave Synthesis of High-flux NaY zeolite Membranes in Fluoride Media

Na Hu[a], Yihong Zheng[a], Zhen Yang[a], Rongfei Zhou*[a,b], Xiangshu Chen*[a]

Received (in XXX, XXX) Xth XXXXXXXXX 20XX, Accepted Xth XXXXXXXXX 20XX

DOI: 10.1039/b000000x

High-flux NaY zeolite membranes were synthesized using low-cost mullite supports by microwave heating in fluoride media. Pervaporation and vapor permeation performances of these membranes were evaluated at temperature range of 303-383 K. The thickness of NaY zeolite membrane prepared by microwave heating was thinner than that prepared by conventional heating. Six membranes synthesized by microwave heating displayed fluxes of 3.43±0.13 kg/(m^2 h) and separation factors 1360±403 for a 95 wt.% *n*-butanol aqueous solution at 348 K. The water fluxes of these membranes were 70-80% higher than those of NaY membranes prepared by conventional heating. Water fluxes and water/alcohol separation factors of these membranes increased with the increasing kinetic diameter of alcohols for the water/methanol, water/ethanol, water/*i*-propanol and water/*n*-butanol binary mixtures. Separation of water/alcohol mixtures through these high-flux membranes were affected by concentration polarization. Increasing flow rates from 9.5 L/h (Reynolds number=1300, laminar flow state) to 37.8 L/h (Reynolds number=5200, turbulent flow state) at 363 K decreased the polarization boundary layer, and thus increased membrane flux and membrane selectivity by 26% and 23%, respectively.

Introduction

Zeolite membranes have attracted increasing attention for separations of gas and liquid mixtures with industrial importance. Many efforts have been made on various strategies and methods for synthesis of zeolite membranes[1-4]. Hydrothermal synthesis under microwave irradiation, known as microwave heating (MH) synthesis, is an effective approach to synthesize high-quality zeolites and zeolite membranes[5-7]. Compared with conventional heating (CH), MH yielded smaller zeolite crystals with narrower particle size distribution and higher purity[5-7]. So far, several types of zeolite membranes including NaA[7], NaY[9], T[10], and MFI[11] zeolite membranes have been synthesized by MH. Zeolite membranes[1,5,7,9-11] synthesized by MH had higher pervaporation (PV) performance compared with those synthesized by CH. On the other hand, some papers reported that the crystalline product phases obtained by MH differed from that prepared by CH using the same gel precursors[12,13]. For example, Carmona et al.[13] reported that the pure phase VPI-5 was obtained by MH, but the impurity phases such as $AlPO_4$-H2 and $AlPO_4$-H3 appeared in the products in the conventional-heating system.

Hydrophilic NaY zeolite (FAU framework) has higher framework Si/Al ratios of 1.5–3.0 than NaA zeolite (LTA framework) and owns a three-dimensional and 12-ring pore structure with a pore size of 0.74 nm. And thus, NaY zeolite membrane, being considered more chemically stable than NaA zeolite membrane, has been a promising candidate for pervaporative separation of water/organics and organics/organics mixtures[14-16]. Kita *et al.*[14,15] prepared a NaY zeolite membrane by CH with a water flux of 1.59 kg/(m^2 h) and a water/ethanol separation factor of 130 for a 90 wt.% ethanol aqueous solution at 348 K. Zhu *et al.*[9] reported the *in-situ* microwave synthesis of a NaY zeolite membrane and the membrane exhibited water fluxes of ~1.70 kg/(m^2 h) and water/ethanol separation factors of ~10000 for the same mixture. However, most of the present NaY zeolite membranes[4,9,15-18] displayed lower water fluxes than NaA zeolite[19] and chabazite[20,21] membranes.

The above hydrophilic low-silica zeolite crystals and membranes were always prepared using the base (OH^-) as mineralizing agent. Fluorides (F^-) as sole mineralizing agent or the combinative one were reported to accelerate the crystallization of high-silica and all-silica zeolites[22-24,] which have been shown to have the absence of framework defects and the large crystal size. Subsequently, some work has been done on the high-silica and all-silica zeolite beta and MFI membranes successfully prepared in fluoride media[25-27], and the fluoride-mediated membrane showed higher organic/water selectivities as compared those by hydroxide route. In our previous works, we introduced the fluorite route for the synthesis of low-silica zeolites and zeolite membranes such as zeolite T[28], NaY[17], chabazite[29], mordenite[30] and ZSM-5[31]. Zeolite membranes prepared in fluoride media normally had thinner membrane layers and displayed higher dehydration performance than those prepared in the fluoride-free media. In the case of NaY zeolite membranes[17], the addition of ammonium fluoride in gel also effectively suppressed the formation of the impurity phase of P-type zeolite in NaY zeolite layers, by which the synthesis reproducibility was improved.

In this current study, we integrated the advantages of MH and fluorite synthesis techniques for the synthesis of NaY zeolite membranes. These lab-scale NaY zeolite membranes showed higher fluxes than the commercial NaA zeolite membranes[19] with similarly high water/alcohol selectivities for the dehydration of several kinds of alcohols. Vapor permeation performances of these membranes were also investigated.

Experimental

Materials

Porous mullite supports (12 mm in outer diameter, 1.5 mm in thickness, 1.3 μm in average pore size) were purchased from Nikkato Corporation. NaY zeolite seeds (~2.0 μm, Si/Al ratio =1.7), sodium silicate solution (concentrations of SiO_2 and Na_2O by weight of ~26.5% and ~14%, respectively), and ammonium fluoride (purity ⩾98%) were purchased from Sigma-Aldrich Company. Sodium aluminate (Al/NaOH ratio =0.79) was purchased from Wako Pure Chemical. Sodium hydroxide (purity ⩾96%) was purchased from Tianjin Fuchen Chemical. Other reagents such as methanol, ethanol, *i*-propanol and *n*-butanol were of analytical grade and used without any further purification.

Synthesis of NaY zeolite membranes

NaY zeolite membranes were grown hydrothermally on the outside surface of tubular porous mullite supports. The morphology of the mullite support was shown in Fig. S1. The supports were polished with 1000# SiC sandpaper, washed and dried at 338 K overnight. The support was rub-coated with water slurry of NaY zeolite seeds. The slurry was prepared by mixing 5.0 g NaY powders and 20 g water and sonicated for 30 min. All the outside surface of the tubes was rubbed back and forth for a total time of approximately 1.0 min. The seeded tubes were dried at 353 K for 1.0 h. The excessive seeds on the surface were then removed slowly by a cotton swab.

Fluoride-mediated membrane gel was prepared using ammonium fluoride as fluoride source as described previously[17]. In a typical synthesis, 1.9 g sodium aluminate was dissolved into 75 ml 3.2 M sodium hydroxide aqueous solution, and then 60.5 g sodium silicate solution and 75 ml 1.1 M ammonium fluoride aqueous solution were added into the aluminate solution. The resulted membrane gel had a molar composition of $25SiO_2$: $1Al_2O_3$: $22Na_2O$: $990H_2O$: $7.5NH_4F$. The gel was stirred at room temperature for 4 h and stored in a water bath at 303 K overnight. Two seeded support were vertically placed into two Teflon reaction vessels which were filled with membrane gel. Hydrothermal treatment was carried out in a microwave reactor (MDS-10, Shanghai Xinyi Co.) at 373 K for 0-10 h. The frequency and power of the microwave were 2450 MHz and 500 W, respectively. Microwave irradiation was normally not spatially uniform, and a horizontal rotation mode was used to eliminate heating differences in spaces. It is also the sole heating mode for this microwave reactor. The rotation speed was 10 run per minute (RPM) for all synthesizes. After hydrothermal synthesis, the membranes were taken out, washed with running tap water for 30 min and dried at 338 K overnight. PV performances of one of two membranes for 9 batches were listed in Table 1. For comparison, NaY zeolite membranes were synthesized by CH under the same synthesis procedure in our previous work[17].

Characterization

Zeolite phases of the as-synthesized membranes were verified by X-ray diffraction (XRD, Rigaku UItima IV) with Cu-Kα radiation. The step size was 0.02^o (2θ) with a scan rate of 4.0^o/min between 5 and 45^o (2θ). The surface and cross-sectional morphologies of the zeolite membranes were examined by field emission scanning electron microscopy (FE-SEM, Hitachi SU-8020). ^{19}F MAS NMR spectra of the powders were also collected on a Bruker Advance III 400 WB at 376.4 MHz with 22 kHz magic angle spinning, 4 μs pulses, 10 s recycle delay and 4.96 scans. $CFCl_3$ was used as chemical shift reference.

PV performances of NaY zeolite membranes were tested in a batch mode as shown in Fig. 1a. One end of the membrane tube was sealed using a solid glass column. The other end was connected with vacuum line using silicone tubes. Membrane tube was immersed into alcohol aqueous solutions in a 3 L flask. A certain of water and alcohol was added in the flask after each 0.5 h to keep the feed concentration constant. The magnetic stirring at 1000 rpm eliminated the concentration differences between membrane surface and the bulk solution. Feed temperature was controlled at the range of 303-348 K by a water bath. The permeate vapor across the inner tube was collected in a trap to determine permeation flux J/kg/(m^2 h) and separation factor (α). The separation factor is determined as $\alpha=(Y_A/Y_B)/(X_A/X_B)$, where X_A, X_B, Y_A, and Y_B denote the mass fractions of components A (water) and B (alcohols) in the feed and permeation sides, respectively. Composition analysis of the feed and permeate were performed using a gas chromatograph (Shimadzu GC-14C) equipped with a TCD detector.

Vapor permeation (VP) experiments were carried out using an apparatus illustrated in Fig. 1b in a continuous mode. The feed solution was pumped into a heater for heating to a given temperature and introduced into the stainless steel module, and then circulated to the feed tank after cooling through a water condenser. Operation temperature was kept constant using an oven and vapour pressure was set at 0.12 MPa (absolute pressure) by a pressure regulator. The effect of concentration polarization on membrane performance was investigated by changing flow rate. The Reynolds number (N_{Re}) which represents the state of turbulence in membrane modules is described as $N_{Re}=De\rho V/\eta$, where De is the equivalent diameter, ρ is the density of feed vapor, V is the velocity of feed vapor, η is the viscosity. The equivalent diameter for the present annulus type tubular module is the difference between the outer diameter of membrane tube (D_1) and the inner diameter of module tube (D_2)[15]. Composition analysis, the calculations of the flux and separation factor were the same as those in PV test.

Results and Discussion

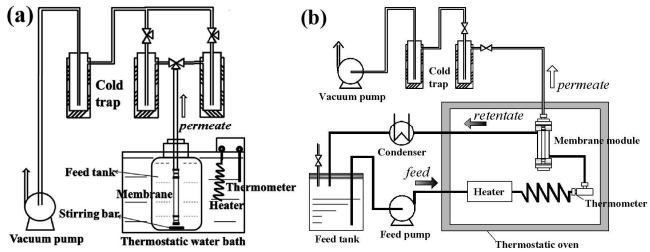

Fig. 1. Schematic illustration of (a) PV test apparatus and (b) VP test apparatus.

Membrane morphologies

Fig. 2 shows SEM images of NaY zeolite membranes prepared by MH (namely MH membrane) for different crystallization time at 373 K. NaY zeolite membrane prepared for a crystallization period of 3.5 h (as shown in Figs. 2a and 2b) shows a membrane-like phase packed loosely with small crystals. Obvious pin-pore defects were seen in their SEM images. Fig. 2c indicates that the support surface was fully coated with zeolite crystals after 5-h synthesis. The grains with particle size of 1-3 μm consisted of hundreds of nanosized NaY crystals. The uniformity of zeolite layers increased with synthesis time, as shown in Figs. 2a and 2c. The cross-sectional views in Figs. 2b and 2d indicate that membrane thickness increases from 2 μm to 4 μm as synthesis time increases from 3.5 h to 5.5 h. When synthesis time increased to 7.5 h, the membrane thickness increased to ~7 μm (as shown in Fig. S2) and resulted into a lower flux (as shown in Table 1). Compared with our previous NaY membranes prepared by CH with or without fluoride[17,32], the surface crystals of the membrane by MH in this study were more uniform and 4-6 times smaller than the previous crystals. Park et al.[33] gave their explanation for the formation of uniform AlPO-11 crystals by MH: The induction of microwave irradiation caused the rotation of the normal H-bonded water molecules by ion oscillation and dipole rotation, and the destruction of the hydrogen bridges produced isolated active water molecules which were considered to have higher potential to dissolve the gel than normal water. The increased dissolution of the gel yielded more nuclei in a short period, and resulted in the relatively uniform and small crystals compared with that by CH.

EDX characterization showed that Si/Al ratio of typical MH membrane (M8) was around 1.6, which was a little lower than that of our previous NaY zeolite membranes synthesized by conventional heating (namely CH membrane)[17] (Si/Al=1.9). MH membrane (M9) had 2/3 membrane thickness and 1.8 times water fluxes (as shown in Table 2), compared with our previous CH membrane[17]. Membrane flux for MH membrane increased by 80%, which was beyond the contribution of the decrease of membrane thickness (~1/3 reduction). Lower Si/Al ratio for the MH membrane increased membrane hydrophilicity[30], which was also responsible for the increased water flux. Synthesis time by MH in this study was just a little lower than that by CH[17,32]. In contrast, it was shortened when CH was replaced with MH to a large extent in some literatures[10,12,34,35]. To make the microwave irradiation for the autoclaves uniform, we used the horizontal rotation mode. The crystallization rate of zeolites and zeolite membranes[36-38] was normally slower in the rotation mode than that in the static mode (*i.e.* our hydrothermal synthesis by CH). The negative effect of the rotation mode on crystallization rate was mainly compensated by the positive effect of MH. And thus, synthesis time for NaY zeolite membrane by MH in this study was not shortened largely in comparison with that for our previous membrane by CH[17] (optimized synthesis time of 5.5 h).

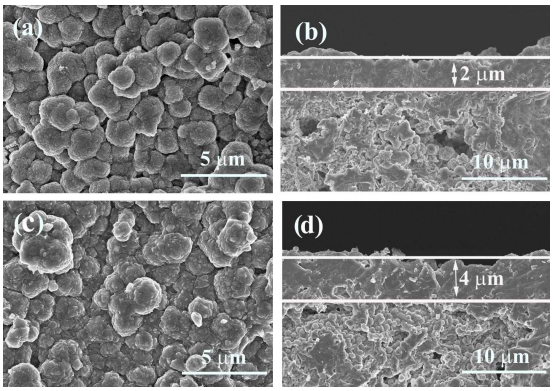

Fig. 2. Surface and cross-sectional SEM images of zeolite membranes synthesized by MH for 3.5 h (a and b) and 5.5 h (c and d).

Role of fluoride

The location of fluorine anions in zeolite crystals is important to understand the effect of fluorine anion on zeolite crystallization. Fluorine generally takes four kinds of the location in zeolite crystals[22-24], including, five-coordinated to silicon, as an ion pair in zeolite channel, in a small cage and out of framework. ^{19}F MAS NMR characterization supplied some evidences for the location of fluorine anions as shown in Fig. S3. The crystals for NMR test were obtained by peeling off the crystals from NaY zeolite membranes prepared by MH and in fluoride media after membrane treatment using liquid nitrogen. No peaks were found in the ^{19}F MAS NMR spectra, suggesting that fluorine anion is out of NaY crystal framwork[39].

We consider that the fluorine precursor in gel affect gel dissolution and nucleation processes. Firstly, fluoride anions as mineralizing agent dissolve silicon precursor to be SiF_6^{2-}[17,39] and then to be $Si(OH)_4$ by hydrolysis, and thus fluorine anion recycled for the dissolution of membrane gel. At the primary stage of nucleation, some fluorine anions are considered to be packed into the sodium hydrates by charge balance when sodium hydrates arrange the nuclei as structural directing agent. The density of nuclei increases as the nucleation undergoes. Because of the repulsive interaction between F^- and AlO_2^-, the high density of negative charge in NaY framework results into the fluoride anion out of NaY framework. We consider that fluorine anions decrease the gismondine (GIS, NaP zeolite) framework more than that of FAU (NaY zeolite) framework since GIS phase framework requires higher AlO_2^- density (~25% higher than FAU framework in our system). Therefore, the addition of a certain fluoride salts suppressed the formation of GIS topology NaP zeolite in competitive growth of FAU/GIS phases.

Separation properties of different alcohols aqueous solutions

Table 1 shows PV performance of NaY zeolite membranes prepared by MH with different synthesis time for a 95 wt.% *n*-butanol aqueous solution at 348 K. Water/*n*-butanol separation

factor increased when synthesis time varied from 3.5 h to 6.5 h, indicating that the intergrowth of the membrane was improved. When synthesis time increased to 9 h, the impurity phase of GIS topology NaP zeolite occurred in the zeolite layers by MH (Fig. S4), which resulted in the decrease of separation factor (α=400). Six NaY zeolite membranes (M3, M5-9) were prepared under optimized synthesis condition. The membranes displayed fluxes of 3.43±0.13 kg/(m^2 h) and separation factors 1360±403, and the deviations of fluxes and separation factors were 4% and 32%, suggesting that our membrane synthesis had a good reproducibility.

Table 1. PV performances for a water/*n*-butanol (5/95 wt.%) mixture at 348 K through NaY membranes prepared in fluoride media by MH with different synthesis time.

Membrane[a] No.	Synthesis time (h)	PV performance	
		J_{total}kg /(m^2 h)	$\alpha_{water/n\text{-butanol}}$
M1	3.5	/	/
M2	4.5	3.82±0.12	560±48
M3	5.5	3.46±0.31	990±436
M4	7.5	2.81±0.11	1000±141
M5	5.5	3.44±0.24	1200±139
M6	5.5	3.23±0.29	2000±992
M7	5.5	3.38±0.12	1100±280
M8	5.5	3.60±0.23	1000±422
M9	5.5	3.52±0.12	1500±285

[a]membrane gel composition: 25SiO_2: 1Al_2O_3: 22Na_2O: 990H_2O: 7.5NH_4F.

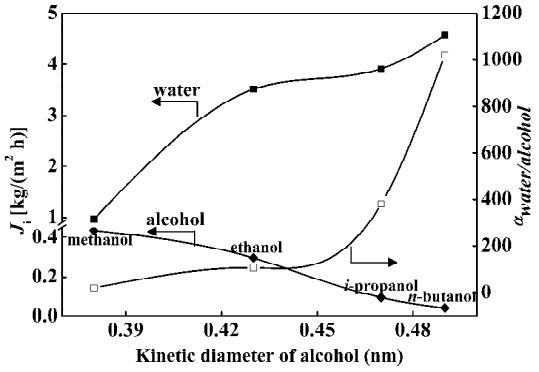

Fig. 3. PV performance as a function of kinetic diameters of alcohols for the alcohol aqueous solutions through NaY zeolite membrane (M9) synthesized by MH. Closed keys: the partial flux of water or alcohol; open keys: the water/alcohol separation factor.

PV performance of MH membrane (M9) was evaluated in four alcohol aqueous systems: methanol, ethanol, *i*-propanol and *n*-butanol. Fig. 3 shows the total flux and water/alcohol separation factor of this membrane as a function of the kinetic diameter of alcohols. All the binary mixtures contained 10 wt.% water and the temperature was 348 K, except for water/methanol mixture, where the temperature was 333 K. Water was preferentially permeated through NaY zeolite membranes over alcohols in these binary mixtures because of its hydrophilic property. Flux and water/alcohol selectivity of this membrane increased with the increasing kinetic diameter of alcohol molecules for the four mixtures. It could be attributed to the differences in adsorption and diffusion abilities of alcohol molecules in zeolite channels. The polarity of the alcohol molecules decreases with the increase of the carbon number in alcohol molecules, resulting in the decrease in adsorption amount over hydrophilic zeolites. The simulated and experimental adsorption capacities of adsorbents on NaA[40,41] and NaY[14] zeolite powders were in the order: water> methanol> ethanol> *i*-propanol. On the other hand, the simulation results[40] showed that the effects of the size and steric hindrance of the diffusing molecules on diffusivity were significant. The diffusivities of water, methanol, and ethanol molecules in NaA zeolite channels decreased by one order of magnitude and were in the order: water> methanol> ethanol[40]. These analyses on the adsorption and diffusion of molecules over hydrophilic zeolites indicated that smaller alcohol molecule was more mobile in permeating through NaY zeolite channels. However, the diffusion of the alcohol molecule always inhibited the permeation of water (the most mobile specie) by at least one order of magnitude. And therefore, the smaller alcohol that easily adsorbed in the zeolite pores greatly prevented the diffusion of faster-permeating water. Meanwhile, the diffusion of water molecules increased more the diffusion of the smaller alcohol molecules. That is, the water flux and water/alcohol selectivity in water/alcohol binary mixtures increased with the increasing kinetic diameter of alcohols. Accordingly, NaA[41] and previous NaY[17] zeolite membranes showed the same dependence of flux and water/alcohol selectivity with alcohol molecular size.

Effects of feed concentration and temperature

Fig. 4 shows feed concentration dependence of PV performance of MH membrane (M9) towards water/*n*-butanol and water/ethanol binary mixtures at 348 K, respectively. In water/*n*-butanol system (Fig. 4a), water flux of this membrane decreased from 5.22 kg/(m^2 h) to 3.47 kg/(m^2 h) but *n*-butanol flux increased from 0.036 kg/(m^2 h) to 0.044 kg/(m^2 h), as *n*-butanol concentration increased from 80 wt.% to 95 wt.%. The corresponding water/*n*-butanol separation factor increased from 500 to 1500 because the decrease rate of water/*n*-butanol ratio in permeate side was lower than that in feed side. Compared with CH membrane[17], this membrane had 70-80 % higher water fluxes and a little higher water/*n*-butanol separation factors. Similar to water/*n*-butanol system, water flux decreased but water/ethanol separation factor increased with the increase of ethanol concentration in water/ethanol system (Fig. 4b). In the case of ethanol concentration of 90 wt.%, water flux and water/ethanol separation factor of this membrane were 3.44 kg/(m^2 h) and 107, respectively.

Fig. 5 shows the feed temperature dependence of PV performance of the MH membrane (M9) towards 95 wt.% *n*-butanol and 90 wt.% ethanol aqueous mixtures, respectively. For either water/ethanol or water/*n*-butanol system, water and alcohol fluxes of this membrane increased with the increase of feed temperature. The increase rates of *n*-butanol fluxes of this membrane were higher than those of the corresponding water fluxes, which led to the decrease of water/*n*-butanol separation factors with temperature. In contrast, the increase rates of ethanol fluxes of this membrane were almost the same with those of the corresponding water fluxes, which resulted that water/ethanol separation factors were independent of temperature.

The flux through a microporous membrane can be described by Maxwell-Stefan surface diffusion:[42]

$$J = \frac{\rho q_{sat} D_{MS}}{L} \ln \frac{1-\theta_p}{1-\theta_f} \quad \text{.....(1)}$$

where, ρ is the zeolite density, L the effective thickness of the membrane, q_{sat} the saturation coverage and θ_f and θ_p are the fractional coverages in the feed and permeate. The coverage-independent Maxwell-Stefan diffusivity, D_{MS}, is given by

$$D_{MS} = D_{MS_0} \exp \frac{-E}{RT} \quad \text{.....(2)}$$

where E is the activation energy of diffusion. Combining Eqs. (1) and (2), yields the flux dependence of temperature.

$$J = \frac{\rho q_{sat} D_{MS_0}}{L} \exp \frac{-E}{RT} \ln \frac{1-\theta_p}{1-\theta_f} \quad \text{.....(3)}$$

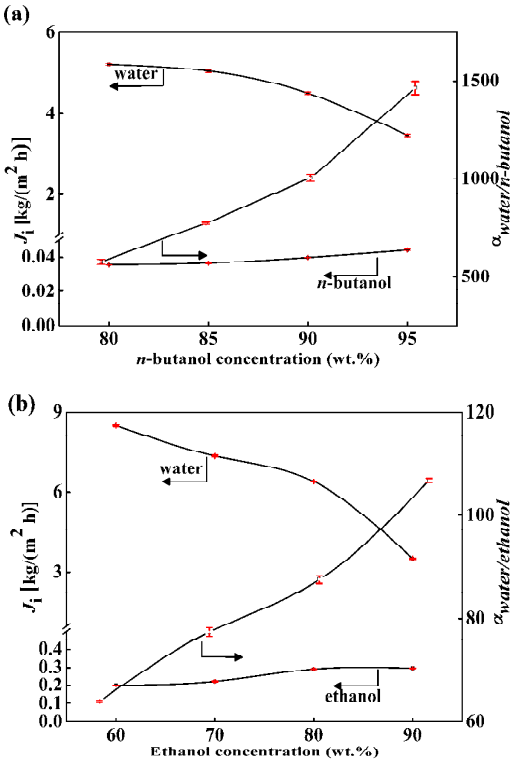

Fig. 4. PV performance as a function of feed concentration for the (a) *n*-butanol and (b) ethanol aqueous solutions at 348 K through NaY zeolite membrane (M9) synthesized by MH, respectively. Closed keys: the partial flux of water or alcohol; open keys: the water/alcohol separation factor.

According to Eq. (3), as temperature increases, activated diffusion increases the flux. Four trends of the inserted figures in Figs. 5a and 5b show the Arrhenius type plots (ln J versus 1000/T) using MH membrane (M9) and our previous CH membrane[17], respectively. The linear trends in the plots indicate that the fluxes in water/*n*-butanol and water/ethanol systems depend mainly on the diffusion other than the coverage-induced adsorption. The activation energies for water permeation through MH membrane (M9) were lower than those through CH membrane in water/*n*-butanol and water/ethanol systems, suggesting that the permeation of water molecule through MH membrane (M9) was easier than that through CH membrane. And therefore, MH membranes displayed higher water flux.

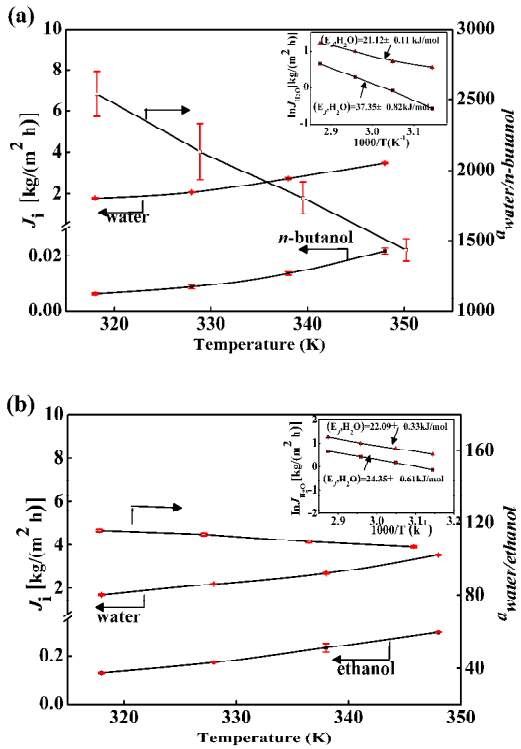

Fig. 5. PV performance as a function of feed temperature for a (a) 95 wt.% *n*-butanol and (b) 90 wt.% ethanol aqueous solution through NaY zeolite membrane (M9) synthesized by MH, respectively. Closed keys: the partial flux of water or alcohol; open keys: the water/alcohol separation factor. The insets in Figs. 5a and 5b are Arrhenius type plots (ln J versus 1000/T) of H_2O for the two mixtures using MH membrane M9 (▲, top line in the inserted Figure) and our previous CH membrane[17] (■, bottom line in the inserted Figure), respectively.

Vapor permeation performance

Fig. 6 shows the VP performances through MH membrane (M9) at 363 K as a function of flow rate of feed vapor. At a low flow rate of 9.50 L/h (Reynolds number=1300), water flux and the water/*n*-butanol separation factor were 4.68 kg/(m^2 h) and 680, respectively, which were lower than our prediction based on PV results in Fig. 3a. Water flux increased to 5.94 kg/(m^2 h) and *n*-butanol flux kept constant when flow rate increased to 37.80 L/h (Reynolds number=5200). Similar to VP performance at 363 K, flux and water/*n*-butanol selectivity of the same membrane at 383 K increased with flow rate, as shown in Fig. S5. It suggested that concentration polarization affected separation performance of NaY zeolite membrane. The faster-permeating water was depleted near the membrane surface because it could not diffuse fast enough from the bulk phase under the laminar flow condition (Reynolds number=1300). When flow rate increased by a factor of 2 (beyond laminar flow), the polarization boundary layer decreased, and water flux and separation factor increased by 21% and 13%, respectively. The increase rate of flux in Reynolds number range of 3900-5200 (turbulent-flow range) was slower than that in the range of 1300-2600 (laminar-flow range) as

shown in Fig. 6. For the actual application of dehydration using the outside membrane, the flow rate and the baffle structure

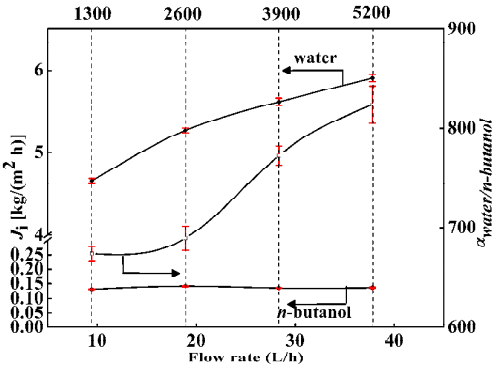

should be optimized to reduce the polarization boundary layer.

Fig. 6. VP performance of MH membrane (M9) as a function of feed flow rate for 95 wt.% *n*-butanol aqueous solution at 363 K. Closed keys: the partial flux of water or alcohol; open keys: the water/alcohol separation factor.

Fig. 7 shows temperature dependence of permeation fluxes through MH membrane (M9) for a 95 wt.% *n*-butanol aqueous solution by an Arrhenius plot (ln *J* versus 1000/T). The feed was vapor state and Reynolds number was around 4000 to reduce the effect of concentration polarization. According to the Arrhenius equation, E_J can be evaluated from the slope of the plot of ln *J* versus 1000/T. The H_2O and alcohol activation energies ($E_{J,\ H2O}$ and $E_{J,\ n\text{-butanol}}$) were 22.41 and 42.70 kJ/mol, respectively. Activation energy for water was much smaller than that for *n*-butanol. It is the reason why water molecule permeates faster than *n*-butanol molecule. Similar to this NaY zeolite membrane, other NaA[41] and NaY[15] zeolite membranes had lower activation energy for water than that for alcohol, resulting in water-selective

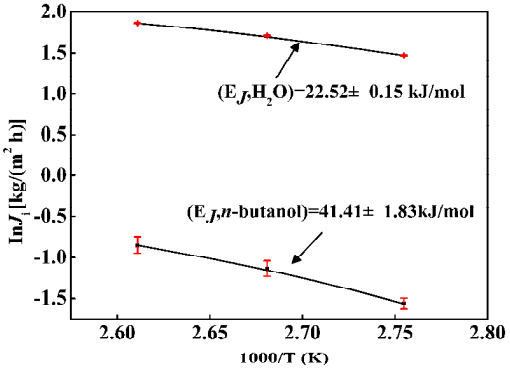

permeation.

Fig. 7. Arrhenius type plot (ln J_i vs. 1000/T) through MH membrane (M9) for a 95 wt.% *n*-butanol aqueous solution in VP mode.

Comparison to the literatures

Table 2 shows the PV performance of water/organics through FAU (NaY and NaX) zeolite membranes. The reported FAU zeolite membranes using the symmetric tubular supports[9,14,43] showed the fluxes of 0.10-1.70 kg/(m^2 h) for a 10/90 wt.% water/ethanol mixture at 303-348 K, which was lower than that of the commercial NaA zeolite membranes[19]. Our previous NaY zeolite membranes prepared in fluoride media by CH showed a higher water flux together with a reasonable separation factor[17]. In the current work, we combined the advantages of MH and fluoride synthesis techniques for NaY zeolite membrane preparation, and the resulted membrane had 70-80 % higher fluxes in the dehydrations of bio-alcohols (ethanol and *n*-butanol) than our previous membrane[17]. Moreover, the low-cost symmetric mullite supports we used are suitable for industrial application.

NaA zeolite membranes were more hydrophilic than NaY zeolite membranes and showed higher water selectivity in separation of water/alcohols mixtures. Although out current lab-scale NaY membrane showed ~80% higher water flux for ethanol dehydration than the commercial zeolite NaA membrane[19], very-high-flux NaA zeolite membranes were prepared on a small scale in some groups [44,45]. Wang group[44] prepared NaA zeolite membranes using PES-zeolite ceramic hollow fiber supports by a single *in-situ* hydrothermal crystallization. The membranes showed fluxes of ~5.6 kg/(m^2 h) and water/ethanol separation factor of ~5000 for a 10/90 wt.% water/ethanol mixture at 348 K. Sato et al.[45] reported a NaA zeolite membrane synthesized on an asymmetric alumina support showed a flux of 9.2 kg/(m^2 h) and water/ethanol separation factor of 10000 for the same test conditions.

Table 2. PV performances of NaY membranes prepared in fluoride media for 10/90 wt.% water/alcohols liquid mixtures.

Water/alcohol (A/B)	Heating	T (K)	PV performance		Ref.
			J/[kg/(m^2 h)]	$\alpha_{A/B}$	
water/ethanol	MH	338	1.70	10000	9
	CH	348	1.59	130	14
	CH	303	0.10	100	43
	CH	348	2.12	105	17
	MH	348	3.84	107	This work
water/*n*-butanol	CH	348	2.55	1000	17
	MH	348	4.56	1020	This work

Conclusions

(1) Thin and compact NaY zeolite membranes with high performance were synthesized on low-cost mullite supports by combining the advantages of microwave heating and fluoride route.

(2) The best membrane synthesized by microwave heating had fluxes of 4.56 and 3.84 kg/(m^2 h) and separation factors of 1020 and 109 towards 90 wt.% *n*-butanol and ethanol aqueous solutions at 348 K, respectively. The fluxes of this membrane were ~80% higher than those of NaY zeolite membrane synthesized by conventional heating.

(3) Separation of water/alcohol mixtures through NaY zeolite membranes with high performance was strongly affected by concentration polarization. Increasing flow rates from 9.5 L/h (Reynolds number=1300, laminar flow state) to 37.8 L/h (Reynolds number=5200, turbulent flow state) at 363 K decreased the polarization boundary layer, and thus increased membrane flux by 26% and

membrane selectivity by 23%.

Acknowledgements

The authors are grateful for the financial support of this study from the National Natural Science Foundations of China (No. 20906042 and 21366013).

Notes and references

[a]*Jiangxi Inorganic Membrane Materials Engineering Research Centre, College of Chemistry and Chemical Engineering, Jiangxi Normal University, Nanchang 330022, P.R. China. Fax: +86-791-88120843; Tel: +86-791-88120533; cxs66cn@jxnu.edu.cn (X.-S. Chen)*

[b]*State Key Laboratory of Materials-Oriented Chemical Engineering, College of Chemistry and Chemical Engineering, Nanjing Tech University, Nanjing 210009, P.R. China. Fax: +86-25-83172239; Tel: +86-25-83172261; rf-zhou@jxnu.edu.cn (R.-F. Zhou)*

† *Electronic Supplementary Information (ESI) available: Fig. S1-S5: SEM morphologies of the supports;SEM morphology of membrane prepared for 7.5 h; ^{19}F MAS NMR spectra for MH NaY crystals; XRD partterns for the support, seeded support and membranes; VP permeance of MH membrane (M9) at 383 K. See DOI: 10.1039/c000000x/.*

1. Y. S. Li, H. L. Chen, J. Liu, W. S. Yang, *J. Membr. Sci.*, 2006, **277**, 230-239.
2. M. M. Shahrestani, A. Moheb, M. Ghiaci, *Vacuum*., 2013, **92**, 70-76.
3. A. S. Huang, N.Y. Wang, J. Caro, *J. Membr. Sci.*, 2012, **389**, 272-279.
4. G. Q. Zhu, Y. S. Li, H. L. Chen, J. Liu, W. S. Yang, *J. Mater. Sci.,* 2008, **43,** 3279-3288.
5. Y. S. Li, W. S. Yang, *J. Membr. Sci.*, 2008, **316**, 3-17.
6. R. F. Zhou, S. L. Zhong, X. Lin, N. P. Xu, *Micropor. Mesopor. Mater.*, 2009, **124**, 117-122.
7. Y. S. Li, J. Liu, W. S. Yang, *J. Membr. Sci.*, 2006, **281**, 646-657.
8. C. S. Cundy, *Collect. Czech. Chem. C.*, 1998, **63**, 1699-1723.
9. G. Q. Zhu, Y. S. Li, H. Zhou, J. Liu, W. S. Yang, *J. Membr. Sci.*, 2009, **337**, 47-54.
10. H. Zhou, Y. S. Li, G. Q. Zhu, J. Liu, W. S. Yang, *Sep. Purif. Technol.*, 2009, **65**, 164-172.
11. Z. Tang, S. J. Kim, X. H. Gu, J. H. Dong, *Micropor. Mesopor. Mater.*, 2009, **118**, 224-231.
12. S. H. Jhung, T. Jin, Y. H. Kim, J. S. Chang, *Micropor. Mesopor. Mater.,* 2008, **109,** 58-65.
13. J. G. Carmona, R. R. Clemente, J. G. Morales, *Zeolites,* 1997, **18**, 340-346.
14. Z. Z. Wang, I. Kumakiri, K. Tanaka, X. S. Chen, H. Kita, *Micropor. Mesopor. Mater.*, 2013, **182**, 250-258.
15. H. Kita, K. Fuchida, T. Horita, H. Asamura, K. I. Okamoto, *Sep. Purif. Technol.*, 2001, **25**, 261-268.
16. K. Sato, K. Sugimoto, T. Nakane, *J. Membr. Sci.*, 2008, **319**, 244-255.
17. F. Zhang, L. N. Xu, N. Hu, N. Bu, R. F. Zhou, X. S. Chen, *Sep. Purif. Technol.*, 2014, **129**, 9-17.
18. I. Kumakiri, K. Hashimoto, Y. Nakagawa, Y. Inoue, Y. Kanehiro, K. Tanaka, H. Kita, *Catal. Today.*, 2014, **236**, 86-91.
19. Y. Morigami, M. Kondo, J. Abe, H. Kita, K. Okamoto, *Sep. Purif. Technol.,* 2011, **25**, 251-260.
20. X. S. Li, H. Kita, H. Zhu, Z. J. Zhang, K. Tanaka, K. I. Okamoto, *Micropor. Mesopor. Mater.*, 2011, **143**, 270-276.
21. Y. Hasegawa, C. Abe, M. Nishioka, K. Sato, T. Nagase, T. Hanaoka, *J. Membr. Sci.*, 2010, **364**, 318-324.
22. C. A. Fyle, D. H. Brouwer, A. R. Lewis, J. M. Chezeau, *J. Am. Chem. Soc.*, 2001, **123**, 6882-6891.
23. H. Koller, A. Wölker, L. A. Villaescusa, M. J. Diaz-Cabañas, S. Valecia, M. A. Camblor, *J. Am. Chem. Soc.*, 1999, **121**, 3368-3376.
24. O. Larlus, V. P. Valtchev, *Chem. Mater.*, 2005, **17**, 881-886.
25. M. L. Gualtieri, *Microporous Mesoporous Mater.*, 2009, **117**, 508-510.
26. Y. L. Chen, G. S. Zhu, Y. Peng, X. D. Yao, S. L. Qiu, *Microporous Mesoporous Mater.*, 2009, **124**, 8-14.
27. A. Tavolaro, *Desalination.*, 2002, **147**, 333-338.
28. F. Zhang, Y. H. Zheng, L. L. Hu, N. Hu, M. H. Zhu, R. F. Zhou, X. S. Chen, H. Kita, *J. Membr. Sci.*, 2014, **456**, 107-116.
29. B. Liu, Y. H. Zheng, N. Hu, T. Gui, Y. Q. Li, F. Zhang, R. F. Zhou, X. S. Chen, H. Kita, *Micropor. Mesopor. Mater.*, 2014, **196**, 270-276.
30. R. F. Zhou, Z. L. Hu, N. Hu, L. Q. Duan, X. S. Chen, H. Kita, *Micropor. Mesopor. Mater.*, 2012, **156**, 166-170.
31. M. H. Zhu, I. Kumakiri, K. Tanaka, H. Kita, *Micropor. Mesopor. Mater.*, 2013, **181**, 47-53.
32. R. F. Zhou, Q. Zhang, J. Shao, Z. Z. Wang, X. S. Chen, H. Kita, *Desalination.*, 2012, **291**, 41-47.
33. M. Park, S. Komarneni, *Micropor. Mesopor. Mater.,* 1998, **20**, 39-44.
34. K. Weh, M. Noack, I. Sieber, J. Caro, *Micropor. Mesopor. Mater.*, 2002, **54**, 27-36.
35. V. Sebastian, R. Mallada, J. Coronas, A. Julbe, R. A. Terpstra, R. W. J. Dirrix, *J. Membr. Sci.*, 2010, **355**, 28-35.
36. J. J. Jafar, P. M. Budd, *Micropor. Mater.*, 1997, **12**, 305-311.
37. M. P. Titus, J. Llorens, F. Cunill, R. Mallada, J. Santamaría, *Catal. Today.*, 2005, **104**, 281-287.
38. M. Pera-Titus, M. Bausach, J. Llorens, F. Cunill, *Sep. Purif. Technol.*, 2008, **59**, 141-150.
39. H. M. Kao, Y. C. Chen, *J. Phys. Chem. B*, 2003, **107**, 3367-3375.
40. J. Y. Wu, Q. L. Liu, Y. Xiong, A. M. Zhu, Y. Chen, *J. Phys. Chem. B.*, 2009, **113**, 4267–4274.
41. K. I. Okamoto, H. Kita, K. Horii, K. Tanaka, *Ind. Eng. Chem. Res.*, 2001, **40**, 163-175.
42. S. G. Li, J. L. Falconer, R. D. Nole, *J. Membr. Sci.*, 2004, **241**, 121-135.
43. I. Kumakiri, T. Yamaguchi, S. I. Nakao, *Ind. Eng. Chem. Res.*, 1999, **38**, 4682-4688.
44. Q. Q. Ge, Z. B. Wang, Y. S. Yan, *J. Am. Chem. Soc.*, 2009, **131**, 17056–17057.
45. K. Sato, T. Nakane, *J. Membr. Sci,*, 2007, **301**, 151-161.